Eur. Phys. J. C (2014) 74:2918
DOI 10.1140/epjc/s10052-014-2918-z

THE EUROPEAN PHYSICAL JOURNAL C

Regular Article - Theoretical Physics

Higgs spin determination in the WW channel and beyond

Jessica Frank, Michael Rauch[a], **Dieter Zeppenfeld**

Institute for Theoretical Physics, Karlsruhe Institute of Technology, 76128 Karlsruhe, Germany

Received: 19 November 2013 / Accepted: 21 May 2014 / Published online: 3 June 2014

Abstract After the discovery of the 126 GeV resonance at the LHC, the determination of its features, including its spin, is a very important ongoing task. In order to distinguish the two most likely spin hypotheses, spin-0 or spin-2, we study the phenomenology of a light Higgs-like spin-2 resonance produced in different gluon-fusion and vector-boson-fusion processes at the LHC. Starting from an effective model for the interaction of a spin-2 particle with the SM gauge bosons, we calculate cross sections and differential distributions within the Monte Carlo program VBFNLO. We find that with specific model parameters such a spin-2 resonance can mimic SM Higgs rates and transverse-momentum distributions in $\gamma\gamma$, WW, and ZZ decays, whereas several distributions allow to separate spin-2 from spin-0, independently of the spin-2 model parameters.

1 Introduction

A new, Higgs-like resonance with a mass of about 126 GeV has been discovered by the LHC experiments ATLAS [1] and CMS [2]. A very important ongoing task is now to probe whether this resonance is the Standard Model (SM) Higgs boson [3–7] responsible for electroweak symmetry breaking. Therefore, the determination of its features like its couplings (including its self-couplings), CP quantum number and spin, is currently a very active field of research.

So far, all experimental results suggest that it is indeed the SM Higgs that has been found: The coupling strengths, measured from the rates in different decay channels at ATLAS and CMS, are in good agreement with the SM expectations [8,9]. A pure CP odd state is already strongly disfavored [10–12], and also recent approaches to determine the spin favor spin-0 over specific spin-2 scenarios [9,11–20]. The observation of the resonance in the di-photon decay mode immediately excludes a spin-1 particle due to the Landau–Yang theorem [21,22], leaving spin-2 as an alternative hypothesis to the spin-0 of the Higgs boson. Due to the variety of possible spin-2 models and discriminating variables, there are many phenomenological attempts to distinguish between spin-0 and spin-2 [23–44].

Neglecting P-wave quark–antiquark collisions, a spin-2 resonance can be produced mainly in gluon fusion or vector-boson fusion (VBF), which are also the most important Higgs production channels. The main decay modes for the observation and analysis of the new resonance include $\gamma\gamma$, $W^+W^- \to 2l2\nu$ and $ZZ \to 4l$. Whereas in a previous analysis [23] we have studied the phenomenology of spin-2 resonances in the VBF photon pair-production mode, we now present cross sections for spin-2 resonances in all these processes and show that with a suitable choice of model parameters, spin-2 resonances can approximately reproduce SM Higgs cross sections in all the different channels. We then focus on the phenomenology of spin-2 resonances in the WW channel produced in gluon fusion or VBF and discuss differential distributions, which can be useful to distinguish between a SM Higgs and a spin-2 resonance. Furthermore, alternative spin-0 scenarios are also considered. Our calculations are performed with the Monte Carlo program VBFNLO [45–47] by using an effective Lagrangian approach for a spin-2 (or spin-0) field interacting with the SM gauge bosons. These parametrizations are presented in Sect. 2. After sketching the relevant aspects of our calculation in Sect. 3, we present the results of our analysis in Sect. 4.

2 Spin-2 and spin-0 parametrization

For the analysis of spin-2 resonances in gluon-fusion and vector-boson-fusion processes, we start from an effective Lagrangian ansatz for a spin-2 singlet state which we have already introduced in Ref. [23]. There, we have restricted ourselves to a model for the interaction of a spin-2 particle with electroweak bosons, since only electroweak-boson

[a] e-mail: michael.rauch@kit.edu

fusion was studied. In order to consider also gluon fusion, we enlarge this model by a new term describing the gluonic interaction, $\frac{f_9}{\Lambda} T_{\mu\nu} G_a^{\alpha\nu} G^{a,\mu}{}_{\alpha}$, and we end up with the effective Lagrangian

$$\mathcal{L}_{\text{Spin-2}} = \frac{1}{\Lambda} T_{\mu\nu} (f_1 B^{\alpha\nu} B^{\mu}{}_{\alpha} + f_2 W_i^{\alpha\nu} W^{i,\mu}{}_{\alpha} + 2 f_5 (D^{\mu}\Phi)^{\dagger} (D^{\nu}\Phi) + f_9 G_a^{\alpha\nu} G^{a,\mu}{}_{\alpha}). \tag{2.1}$$

Λ is the characteristic energy scale of the underlying new physics, f_i are variable coupling parameters, $B^{\alpha\nu}$, $W_i^{\alpha\nu}$, and $G_a^{\alpha\nu}$ are the field strength tensors of the SM gauge bosons and D^{μ} is the covariant derivative

$$D^{\mu} = \partial^{\mu} - i g W_i^{\mu} \frac{\sigma^i}{2} - i g' Y B^{\mu}. \tag{2.2}$$

Φ is a scalar doublet field with vacuum expectation value $v/\sqrt{2} = 174$ GeV. The mass of the spin-2 particle is taken as a free parameter.

The Lagrangian (2.1) yields five relevant vertices, which involve two gauge bosons and the spin-2 particle T, namely TW^+W^-, TZZ, $T\gamma\gamma$, $T\gamma Z$, and Tgg. The corresponding Feynman rules are:

$$\begin{aligned}
TW^+W^- &: \frac{2 i f_2}{\Lambda} K_1^{\alpha\beta\mu\nu} + \frac{i f_5 g^2 v^2}{2\Lambda} K_2^{\alpha\beta\mu\nu},\\
TZZ &: \frac{2i}{\Lambda}(f_2 c_{\text{w}}^2 + f_1 s_{\text{w}}^2) K_1^{\alpha\beta\mu\nu} + \frac{i f_5 v^2}{2\Lambda}(g^2 + g'^2) K_2^{\alpha\beta\mu\nu},\\
T\gamma\gamma &: \frac{2i}{\Lambda}(f_1 c_{\text{w}}^2 + f_2 s_{\text{w}}^2) K_1^{\alpha\beta\mu\nu},\\
T\gamma Z &: \frac{2i}{\Lambda} c_{\text{w}} s_{\text{w}} (f_2 - f_1) K_1^{\alpha\beta\mu\nu},\\
Tgg &: \frac{2 i f_9}{\Lambda} \delta^{ab} K_1^{\alpha\beta\mu\nu},
\end{aligned} \tag{2.3}$$

where c_{w} and s_{w} denote the cosine and sine of the Weinberg angle, v is the vacuum expectation value of the Higgs field and the two different tensor structures are given by

$$\begin{aligned}
K_1^{\alpha\beta\mu\nu} &= p_1^{\nu} p_2^{\mu} g^{\alpha\beta} - p_1^{\beta} p_2^{\nu} g^{\alpha\mu} - p_2^{\alpha} p_1^{\nu} g^{\beta\mu} + p_1 \cdot p_2 \, g^{\alpha\nu} g^{\beta\mu},\\
K_2^{\alpha\beta\mu\nu} &= g^{\alpha\nu} g^{\beta\mu}.
\end{aligned} \tag{2.4}$$

The indices μ and ν correspond to the spin-2 field (which is symmetric in the Lorentz indices), α is the index of the first gauge boson, whose incoming four-momentum is denoted as p_1 and β is the index of the second one with four-momentum p_2. a and b are the color indices of the two gluons. The propagator of the spin-2 field is the same as in Ref. [23], yet enlarged by an additional gluonic contribution to the decay width.

The graviton-inspired 2_m^+ scenario, which is mostly studied by the experimental groups [17–20], is a special case of our model. There, the strength of the different operators is equal, $f_1 = f_2 = f_5 = f_9$. As the operators lead to different Lorentz structures, this can a priori have a significant impact on the studied distributions. This aspect is important compared with the log-likelihood values for the Higgs and the 2_m^+ scenario obtained from the measurements. Only in the diphoton channel, where the K_2 structure does not contribute, do the experimental results apply much more directly. There, however, the two experiments find quite different results: while ATLAS excludes the 2_m^+ scenario at a confidence level corresponding to 3 standard deviations, CMS in contrast even prefers the spin-2 hypothesis over the spin-0 one and disfavors spin-0 almost at the 95 % confidence level. For the WW and ZZ final state both experiments prefer spin-0 over spin-2, but the variable relative contribution of the K_1 and K_2 structures raises the question of applicability to our more general model, which therefore should be studied in its own right.

Since the present spin-2 model is based on an effective Lagrangian approach, it violates unitarity above a certain energy scale. In order to parametrize high-energy contributions beyond this effective model, we use a form factor which is multiplied with the amplitudes:

$$F_{\text{Spin-2}} = \left(\frac{\Lambda_{\text{ff}}^2}{|p_1^2| + \Lambda_{\text{ff}}^2} \cdot \frac{\Lambda_{\text{ff}}^2}{|p_2^2| + \Lambda_{\text{ff}}^2} \cdot \frac{\Lambda_{\text{ff}}^2}{|k_{\text{sp2}}^2| + \Lambda_{\text{ff}}^2} \right)^{n_{\text{ff}}}. \tag{2.5}$$

Here, p_1^2 and p_2^2 are the squared invariant masses of the initial gauge bosons and k_{sp2}^2 is the squared invariant mass of an s-channel spin-2 particle. The energy scale Λ_{ff} and the exponent n_{ff} are free parameters, describing the scale of the cutoff and the suppression power, respectively.

Anomalous couplings of a Higgs boson to electroweak bosons can also be described by an effective Lagrangian approach [45–49]:

$$\begin{aligned}
\mathcal{L}_{\text{Spin-0}} = \frac{1}{\Lambda_5} H \Big(& g_{5e}^{HWW} W_{\mu\nu}^{+} W_{-}^{\mu\nu} + g_{5o}^{HWW} \widetilde{W}_{\mu\nu}^{+} W_{-}^{\mu\nu}\\
& + \frac{g_{5e}^{HZZ}}{2} Z_{\mu\nu} Z^{\mu\nu} + \frac{g_{5o}^{HZZ}}{2} \widetilde{Z}_{\mu\nu} Z^{\mu\nu}\\
& + \frac{g_{5e}^{H\gamma\gamma}}{2} A_{\mu\nu} A^{\mu\nu} + \frac{g_{5o}^{H\gamma\gamma}}{2} \widetilde{A}_{\mu\nu} A^{\mu\nu}\\
& + g_{5e}^{HZ\gamma} Z_{\mu\nu} A^{\mu\nu} + g_{5o}^{HZ\gamma} \widetilde{Z}_{\mu\nu} A^{\mu\nu} \Big).
\end{aligned} \tag{2.6}$$

$\widetilde{V}_{\mu\nu}$ are the dual field strength tensors $\widetilde{V}_{\mu\nu} = \frac{1}{2}\varepsilon_{\mu\nu\rho\sigma} V^{\rho\sigma}$, Λ_5 is the energy scale of the underlying new physics and $g_{5e(o)}^{HVV}$ denote the free coupling parameters corresponding to $\mathcal{CP}$-even (-odd) operators.

Analogous to the spin-2 case, a form factor can be multiplied with the vertices to modify the high-energy behavior:

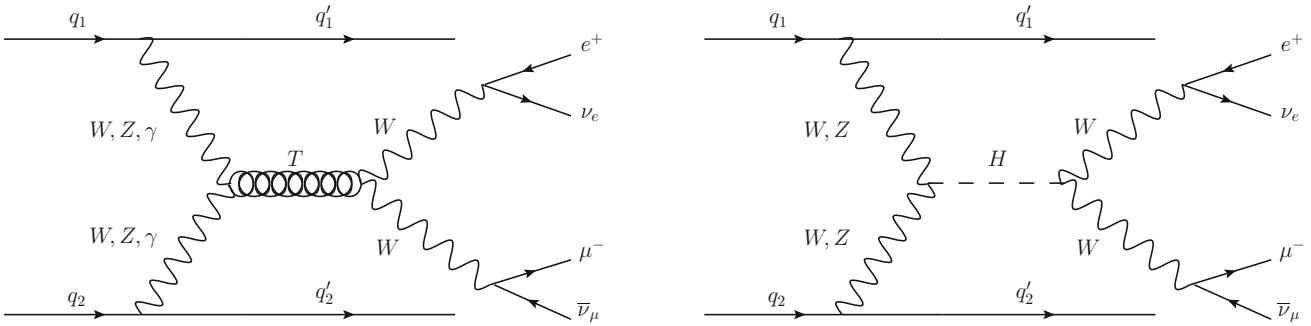

Fig. 1 Tree-level Feynman graphs of the VBF process $pp \to W^+W^- jj \to e^+ \nu_e \mu^- \overline{\nu}_\mu jj$. *Left hand side* via a spin-2 resonance, *right hand side* via a Higgs resonance

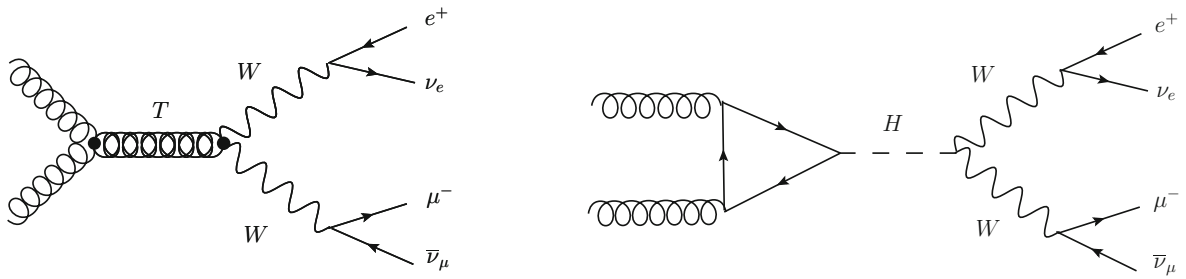

Fig. 2 Feynman graphs of the process $gg \to W^+W^- \to e^+ \nu_e \mu^- \overline{\nu}_\mu$. *Left hand side* via a spin-2 resonance, *right hand side* via a Higgs resonance

$$F_{\text{Spin}-0} = \frac{\Lambda_{\text{ff}_0}^2}{|p_1^2| + \Lambda_{\text{ff}_0}^2} \cdot \frac{\Lambda_{\text{ff}_0}^2}{|p_2^2| + \Lambda_{\text{ff}_0}^2}, \tag{2.7}$$

with Λ_{ff_0} describing the energy scale of the cutoff.

3 Elements of the calculation

In the present analysis, we study the characteristics of Higgs and spin-2 resonances produced in gluon fusion and vector-boson fusion, which decay into $\gamma\gamma$, $W^+W^- \to l^+\nu l^-\bar{\nu}$ or $ZZ \to 4l$. To this end, we use the parton-level Monte Carlo program VBFNLO [45–47].

The analysis of Higgs and spin-2 resonances in vector-boson fusion is performed with NLO QCD accuracy. For the photon pair-production channel, our calculation is described in detail in Ref. [23], and we follow the same procedure also for the VBF WW and ZZ decay mode. In all cases, we only consider resonant diagrams, which are illustrated in Fig. 1 for the WW channel at tree-level. Thereby, Higgs and spin-2 production are implemented as two separate processes in order to compare the characteristics of both cases. The SM continuum contributions are omitted, as interference effects are small due to the narrowness of the Higgs or spin-2 resonance. Since the resonance is part of the electroweak sub-process, the NLO QCD corrections for the spin-2 case can be adapted from the existing calculation for VBF Higgs production [50]. The real-emission contributions are obtained by attaching an external gluon to the two quarks lines of Fig. 1 in all possible ways, which also comprises quark–gluon initiated sub-processes. Due to the color-singlet structure of VBF processes, the virtual corrections only comprise Feynman diagrams with a virtual gluon attached to a single quark line, which gives rise to vertex and quark self-energy corrections.

Gluon-induced di-boson-production processes [51–57] are available in VBFNLO at leading order, i.e. at the one-loop level for Higgs boson production, including anomalous Higgs couplings to electroweak gauge bosons for the decays. We have extended these implementations by spin-2-resonant processes in the effective Lagrangian approach, again omitting non-resonant diagrams. The contributing graphs are exemplified in Fig. 2 for WW production. In the spin-2-resonant process $gg \to ZZ \to 4l$, we also include intermediate virtual photons leading to a leptonic final state. To account for higher-order QCD corrections up to NNLL, which have sizable effects for Higgs production via gluon fusion [58–75], we multiply the LO cross sections calculated with VBFNLO with a K-factor of 2.6,[1] which was obtained by comparing with the value given in Ref. [76] (removing NLO EW corrections of about 5 % [77] included therein). Thereby, we assume that higher-order QCD corrections for

[1] This K-factor is rather high due to the scale choice $\mu_F = \mu_R = m_h$ for gluon fusion (see Sect. 3.1). With $\mu_F = \mu_R = m_h/2$, it would be only ≈ 2.1, because of a higher LO cross section.

spin-2-resonant production in gluon fusion are the same as for Higgs production, since the operator structure of the Tgg coupling, $T_{\mu\nu}G_a^{\alpha\nu}G^{a,\mu}{}_{\alpha}$, is analogous to the one of the effective Hgg coupling, $HG_a^{\mu\nu}G^a_{\mu\nu}$. This assumption has been tested explicitly in Ref. [78]. There, no changes in shape have been observed between a tree-level and an NLO calculation, both augmented with parton shower, for observables which are insensitive to additional jet radiation. The invariant mass of the two leptons in the WW decay mode, which we will consider later, is an example for that. As higher-order QCD corrections also affect the decay of the spin-2 particle to gluons, we multiply the corresponding partial decay width with the K-factor 1.7, again following results obtained for the $H \to gg$ decay [79–81]. We note that only the assumed ratio of K-factors is relevant for spin-2 phenomenology, since the overall coupling strength of the spin-2 resonance to gluons, f_9/Λ, is a free parameter in our model.

3.1 Input parameters and selection cuts

As electroweak input parameters, we choose $m_W = 80.399$ GeV, $m_Z = 91.1876$ GeV and $G_F = 1.16637 \cdot 10^{-5}\,\text{GeV}^{-2}$, which are taken from results of the Particle Data Group [82]. α and $\sin^2\theta_W$ are derived from these quantities using tree-level electroweak relations. We use the CTEQ6L1 [83] parton distribution functions at LO and the CT10 [84] set at NLO with $\alpha_s(m_Z) = 0.118$. In vector-boson-fusion processes, we set the factorization scale and the renormalization scale to $\mu_F = \mu_R = Q = \sqrt{|q_{\text{if}}^2|}$, where q_{if} is the four-momentum transfer between the respective initial- and final-state quarks. For gluon fusion or quark–antiquark-initiated di-boson-production processes, we use a fixed scale of 126 GeV as factorization and renormalization scale. Jets are recombined from the final-state partons by using the $k_\perp$ jet finding algorithm [85]. If not indicated otherwise, we consider a SM Higgs without anomalous HVV couplings and a spin-2 resonance with couplings $f_1 = 0.04$, $f_2 = 0.08$, $f_5 = 10$, $f_9 = 0.04$ and $\Lambda = 6.4$ TeV. The parameters of the form factor are $\Lambda_{\text{ff}} = 400$ GeV, $n_{\text{ff}} = 3$. These couplings produce rates which closely resemble those for the SM Higgs boson (see Table 1). The mass of the Higgs boson and the spin-2 particle is set to 126 GeV and we assume pp collisions at a center of mass energy of 8 TeV.

Vector–boson-fusion events are characterized by two tagging jets in the forward regions, with decay products of the vector bosons lying in the central-rapidity region between them. By applying the following inclusive VBF cuts, these features can be used to improve the signal-to-background ratio in the VBF channels. The two tagging jets are supposed to lie inside the rapidity range accessible to the detector and to have large transverse momenta:

$$p_{T,j}^{\text{tag}} > 30\,\text{GeV}, \quad |\eta_j^{\text{tag}}| < 4.5. \tag{3.1}$$

They are reconstructed from massless partons of pseudo-rapidity $|\eta| < 5$ and have to be well separated:

$$\Delta R_{jj} \equiv \sqrt{(\eta_{j1} - \eta_{j2})^2 + (\phi_{j1} - \phi_{j2})^2} > 0.7. \tag{3.2}$$

Due to the characteristic VBF kinematics, we require a large rapidity separation and a large invariant mass of the tagging jets,

$$\Delta\eta_{jj}^{\text{tag}} > 4, \quad m_{jj}^{\text{tag}} > 500\,\text{GeV}, \tag{3.3}$$

which have to be located in opposite detector hemispheres,

$$\eta_{j1}^{\text{tag}} \times \eta_{j2}^{\text{tag}} < 0. \tag{3.4}$$

The charged decay leptons (or decay photons, respectively) are supposed to be located at central rapidities, to be well separated from the jets and to fall into the rapidity gap between the two tagging jets:

$$|\eta_l| < 2.5, \quad \Delta R_{lj} > 0.4, \quad \eta_{j,\text{min}}^{\text{tag}} < \eta_l < \eta_{j,\text{max}}^{\text{tag}}. \tag{3.5}$$

Here, l denotes a charged lepton or a photon, depending on the considered process. In the leptonic decay channels, we apply a cut on the invariant mass of two oppositely charged leptons,

$$m_{ll} > 15\,\text{GeV} \tag{3.6}$$

Table 1 Integrated cross sections for a SM Higgs and a spin-2 resonance with couplings $f_1 = 0.04$, $f_2 = 0.08$, $f_5 = 10$, $f_9 = 0.04$ in VBF and gluon fusion (see text for details). The cuts of Sect. 3.1 are applied

Final state	Production mode	Higgs cross sec. (fb)	Spin-2 cross sec. (fb)
$\gamma\gamma$	VBF	0.745	0.864
	Gluon fusion	37.1	35.7
$W^+W^- \to e^+\nu_e\,\mu^-\bar{\nu}_\mu$	VBF	0.662	0.613
	Gluon fusion	30.1	29.6
$ZZ \to e^+e^-\mu^+\mu^-$	VBF	$1.06 \cdot 10^{-2}$	$0.982 \cdot 10^{-2}$
	Gluon fusion	0.468	0.446

and require the transverse momentum of the charged leptons to be

$$\begin{aligned} p_{T,\mathrm{l}} &> 10\,\mathrm{GeV} \quad \text{in the } WW \text{ and} \\ p_{T,\mathrm{l}} &> 7\,\mathrm{GeV} \quad \text{in the } ZZ \text{ mode.} \end{aligned} \tag{3.7}$$

In the di-photon channel, we require

$$p_{T,\gamma} > 20\,\mathrm{GeV}. \tag{3.8}$$

In order to have isolated photons, we apply a minimal photon–photon R-separation,

$$\Delta R_{\gamma\gamma} > 0.4, \tag{3.9}$$

and we impose photon isolation from hadronic activity as suggested in Ref. [86] with separation parameter $\delta_0 = 0.7$, efficiency $\epsilon = 1$, and exponent $n = 1$.

Divergences from t-channel exchange of photons with low virtuality in real-emission contributions are eliminated by imposing an additional cut on the photon virtuality,

$$Q_\gamma^2 > 4\,\mathrm{GeV}^2. \tag{3.10}$$

Analogous to Ref. [87], the precise treatment of this divergence does not appreciably affect the cross section, in particular when VBF cuts are applied.

In the case of gluon fusion, we apply the same cuts on the charged decay leptons as in VBF, with

$$p_{T,\mathrm{l}} > 10\,\mathrm{GeV}, \quad |\eta_\mathrm{l}| < 2.5, \quad m_{\mathrm{ll}} > 15\,\mathrm{GeV} \tag{3.11}$$

for the $W^+W^- \to l^+\nu l^-\bar{\nu}$ decay channel (and also for the di-boson-production background) and

$$p_{T,\mathrm{l}} > 7\,\mathrm{GeV}, \quad |\eta_\mathrm{l}| < 2.5, \quad m_{\mathrm{ll}} > 15\,\mathrm{GeV} \tag{3.12}$$

for $ZZ \to 4l$. In the di-photon decay channel, we again require

$$p_{T,\gamma} > 20\,\mathrm{GeV}, \quad |\eta_\gamma| < 2.5, \quad \Delta R_{\gamma\gamma} > 0.4. \tag{3.13}$$

In order to eliminate unwanted off-shell contributions in phase space regions where some of our approximations fail, we apply an additional cut on the invariant mass of all four final-state leptons (or the two photons, respectively) of ± 10 GeV around the 126 GeV resonance in all gluon-fusion processes.

4 Results

In this section, we compare rates of a SM Higgs and a spin-2 resonance produced in VBF or gluon fusion for $\gamma\gamma$, $W^+W^- \to 2l2\nu$ and $ZZ \to 4l$ decays. Focusing on the WW decay channel, we present differential distributions which can be useful for a spin determination and study the impact of spin-0 and spin-2 model parameters and of next-to-leading order (NLO) QCD corrections in the VBF mode. In the case of gluon fusion, distributions are determined at LO QCD and include a normalization factor $1/\sigma_{\mathrm{LO}}$, while VBF figures are normalized to the NLO cross section. Due to the free coupling parameters f_i of the spin-2 Lagrangian (2.1), cross sections can be tuned such that they mimic those of a SM Higgs within experimental and theoretical uncertainties. This was already shown for VBF photon-pair production in Ref. [23], yet is not only possible for single production and decay modes, but simultaneously for all the channels studied here. In the case of a SM Higgs, the decay to two photons is suppressed compared to WW and ZZ decays, since the $H\gamma\gamma$ coupling is loop-induced. A similar suppression can be achieved in our model by tuning the different couplings f_i: As can be seen from the Feynman rules in Eq. 2.3, the coupling f_5 appears only in the TWW and TZZ vertex, but not in $T\gamma\gamma$ and $T\gamma Z$. By choosing $f_5 \gg f_1$, f_2 the decay to $\gamma\gamma$ can thus be suppressed compared to WW and ZZ. That this is in fact possible for our parameter choice given above is illustrated in Table 1, which shows the integrated cross sections for a SM Higgs and a spin-2 resonance. The statistical errors from the Monte Carlo integration are less than one per mill. The NLO QCD corrections in the VBF channels are quite small for a Higgs and a spin-2 resonance, with K-factors $K = \sigma_{\mathrm{NLO}}/\sigma_{\mathrm{LO}}$ between 1.01 and 1.03. Note that for graviton-like spin-2 models, it is not possible to obtain Higgs-like ratios in such a way [41]. However, the ratio of Higgs and spin-2 rates depends on cuts, e.g. in the WW channel, it changes significantly if additional upper cuts on the invariant di-lepton mass and the azimuthal angle difference of the charged leptons are applied. With the ATLAS Higgs search cuts [88,89] $m_{\mathrm{ll}} < 50\,\mathrm{GeV}$ and $|\Delta\Phi_{\mathrm{ll}}| < 1.8$, the SM Higgs cross section in $gg \to W^+W^- \to e^+\nu_e\,\mu^-\bar{\nu}_\mu$ reduces from 30.1 fb (see Table 1) to 18.2 fb, whereas in the case of spin-2, it is only 11.0 fb instead of 29.6 fb. This feature originates from the spin-dependent lepton kinematics in this channel, as we will discuss later. The width of the spin-2 resonance is far below the experimental resolution. With our default couplings, it is only about 5 keV.

In order to complete the set of decay channels which involve the spin-2 vertices (2.3) and are accessible at the LHC, one should also consider the $Z\gamma$ channel and compare the spin-2 rate with current exclusion limits from LHC Higgs searches [90,91]. With our default couplings $f_1 = 0.04$, $f_2 = 0.08$, $f_5 = 10$, $f_9 = 0.04$, which reproduce SM Higgs cross sections in the $\gamma\gamma$, WW, and ZZ modes, the cross section in $gg \to e^+e^-\gamma$ is 0.143 fb, which is much lower than the one of the SM Higgs (0.771 fb). Cuts for this channel have been chosen as $p_{T,\gamma} > 15\,\mathrm{GeV}$, $p_{T,\mathrm{l}} >$

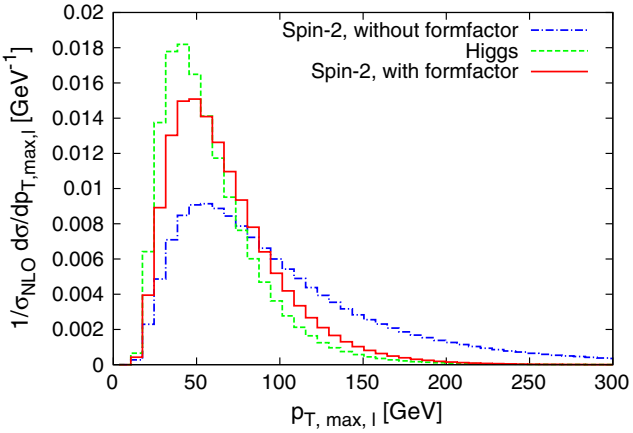

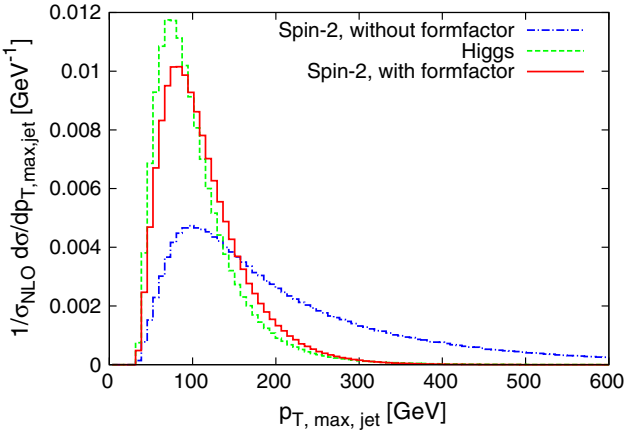

Fig. 3 Transverse-momentum distributions in VBF $W^+W^- \to e^+\nu_e\,\mu^-\,\overline{\nu}_\mu$ events for a SM Higgs and for a spin-2 resonance with couplings $f_1 = 0.04$, $f_2 = 0.08$, $f_5 = 10$, $f_9 = 0.04$, with and without form factor, at NLO QCD accuracy. *Left hand side* p_T of the hardest final-state lepton, *right hand side* p_T of the tagging jet with the largest transverse momentum

10 GeV, $|\eta_l| < 2.5$, $|\eta_\gamma| < 2.5$, $\Delta R_{ll} > 0.4$ and $\Delta R_{l\gamma} > 0.4$. Thus, there is no contradiction with current LHC data. The $Z\gamma$ rate can also be adjusted to the one of the SM Higgs with a slight modification of the spin-2 couplings. Enhancing the cross section in the $Z\gamma$ channel is possible by enhancing the difference of f_1 and f_2, since the Feynman rule of the $T\gamma Z$ vertex in Eq. 2.3 is governed by $f_2 - f_1$. With the parameter choice $f_1 = 0.01$, $f_2 = 0.2$ and all other parameters unchanged, the spin-2-resonant cross section in $gg \to e^+e^-\gamma$ is enhanced to 0.743 fb. Thereby, the spin-2 rate resembles the Higgs rate regardless of cuts on the invariant di-lepton mass, since the ratio of intermediate $Z\gamma$ and $\gamma\gamma$ contributions to $gg \to e^+e^-\gamma$ is similar to the SM Higgs. At the same time, changes to the other results of Table 1 are only moderate, typically at a level of 10 % or less, and the differences to the Higgs cross sections are still well inside the uncertainties of the respective experimental measurements. In the following, we will, however, stick to our original parameter set with a better agreement between Higgs and spin-2 cross sections in the WW final state.

Finally, we have ignored any couplings of the spin-2 particle to fermions. Looking at the branching ratios of the observed resonance into the different final states, one sees that the experimental measurements follow approximately the SM Higgs pattern. The adapted spin-2 couplings of Table 1 exhibit the same pattern: the f_5 term must be much larger than the other ones to obtain the right rates. This also applies to the couplings of a spin-2 resonance to the light fermions. Their effective size cannot be large compared to the SM Higgs value, and therefore their impact can be neglected.

Another question arises whether in the VBF channels a significant fraction of the events could arise from spin-2 emission off a bremsstrahlung gluon. Here a similar argument holds. The effective spin-2 coupling to gluons must be significantly smaller than the coupling to W or Z pairs ($|f_5| \gg |f_9|$ as found in Table 1). Hence radiation off external gluons will be negligible just like in the SM Higgs case.

In Ref. [23], we have shown that in the case of VBF photon-pair production, not only cross sections, but also transverse-momentum distributions of a spin-2 resonance can be adjusted to those of the SM Higgs by choosing the spin-2 form-factor parameters of Eq. 2.5 to be $\Lambda_{\rm ff} = 400$ GeV, $n_{\rm ff} = 3$. Again, this is simultaneously possible for $\gamma\gamma$, WW, and ZZ decays within our set of form-factor parameters (see Fig. 3 for WW). Therefore, transverse-momentum distributions are not sufficient for a spin determination; harder p_T distributions for the spin-2 case without our specific form-factor setting originate from the higher energy dimensions of the couplings in the effective Lagrangian (2.1) instead of being an indicator of the spin. In fact, a similar behavior was found in Ref. [49] for a Higgs boson with anomalous couplings as in Eq. 2.6.

By contrast, the azimuthal angle difference between the two tagging jets was found to be an important variable for the determination of the spin in VBF photon-pair production [23]. This also holds for the WW and ZZ decay channels, with distributions similar to the di-photon case, as illustrated in Fig. 4 for $W^+W^- \to e^+\nu_e\,\mu^-\,\overline{\nu}_\mu$, including different spin-2 coupling parameters and the form factor with $\Lambda_{\rm ff} = 400$ GeV, $n_{\rm ff} = 3$. Note that the parameter choice $f_1 = f_2 = f_5 = 1$ resembles the electroweak part of the graviton scenario, but it cannot reproduce the observed Higgs rates, in contrast to our default choice. Since the $\Delta\Phi_{jj}$ distribution features a clear difference between a SM Higgs and a spin-2 resonance, which is nearly independent of the spin-2 couplings, the form factor, the NLO QCD corrections and the decay mode, it is one of the most important tools to distin-

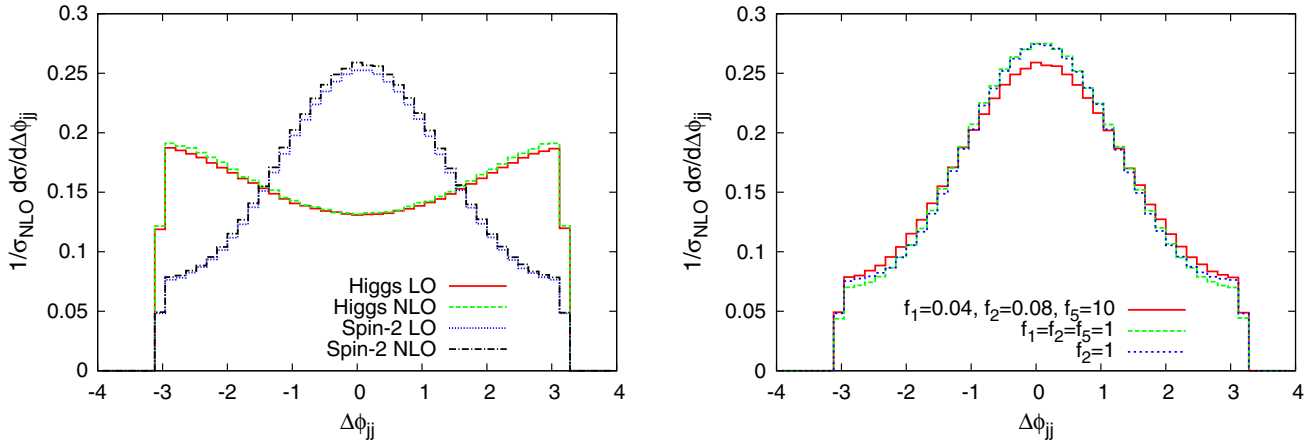

Fig. 4 Azimuthal angle difference of the two tagging jets for $W^+W^- \to e^+\,\nu_e\,\mu^-\,\overline{\nu}_\mu$ in VBF. *Left hand side* SM Higgs and spin-2 resonance with couplings $f_1 = 0.04$, $f_2 = 0.08$, $f_5 = 10$, $f_9 = 0.04$, both at LO and NLO QCD accuracy; *right hand side* spin-2 resonance with different coupling parameters (always including $f_9 = 0.04$) at NLO QCD accuracy

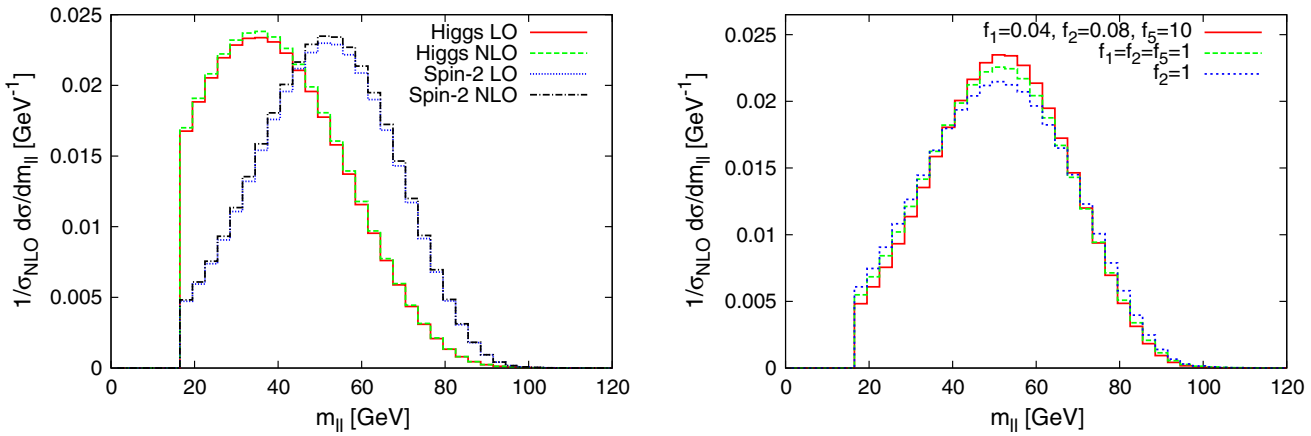

Fig. 5 Invariant mass of the two charged leptons for $W^+W^- \to e^+\,\nu_e\,\mu^-\,\overline{\nu}_\mu$ in the VBF mode. *Left hand side* SM Higgs and spin-2 resonance with couplings $f_1 = 0.04$, $f_2 = 0.08$, $f_5 = 10$, $f_9 = 0.04$, both at LO and NLO QCD accuracy; *right hand side* spin-2 resonance with different coupling parameters (always including $f_9 = 0.04$) at NLO QCD accuracy

guish between spin-0 and spin-2 in VBF. However, the spin-0 distribution is model dependent: anomalous HVV couplings (Eq. 2.6) strongly alter the $\Delta\Phi_{jj}$ distribution [49]. Furthermore, the distribution of the SM Higgs depends on the cuts, e.g. with more stringent lepton p_T cuts in the WW or ZZ mode, it is more central than the one of Fig. 4, which impairs the discriminating power.

In the $W^+W^- \to l^+\nu l^-\bar{\nu}$ decay channel, the invariant mass of the two charged leptons is another variable which is well known to be an indicator of the spin [42]. For a spin-0 resonance, the spins of the two W bosons must be antiparallel, which leads to parallel momenta of the two charged leptons and therefore to a small invariant di-lepton mass. Contrarily, in the spin-2 case, the spins of the W bosons can be parallel, leading to antiparallel lepton momenta and a large invariant di-lepton mass. This is illustrated in Fig. 5 for the VBF mode, which shows that the invariant di-lepton mass is much larger for a spin-2 resonance than for a SM Higgs and nearly independent of the spin-2 coupling parameters and the NLO QCD corrections. Note that these distributions include a cut $m_{ll} > 15$ GeV (see Sect. 3).

The same characteristic difference between a Higgs and a spin-2 resonance also arises in the gluon-fusion mode, which is depicted in Fig. 6. This figure additionally shows the normalized di-boson-production background for comparison, including $q\bar{q} \to W^+W^- \to e^+\,\nu_e\,\mu^-\,\overline{\nu}_\mu$ at NLO QCD accuracy and loop-induced $gg \to W^+W^- \to e^+\,\nu_e\,\mu^-\,\overline{\nu}_\mu$ fermion-box contributions. With an inclusive cross section of around 400 fb, this background exceeds the one of a Higgs or spin-2 resonance significantly, even after placing more stringent search cuts. Since the maximum of the invariant di-lepton mass distribution is nearly at the same position for the

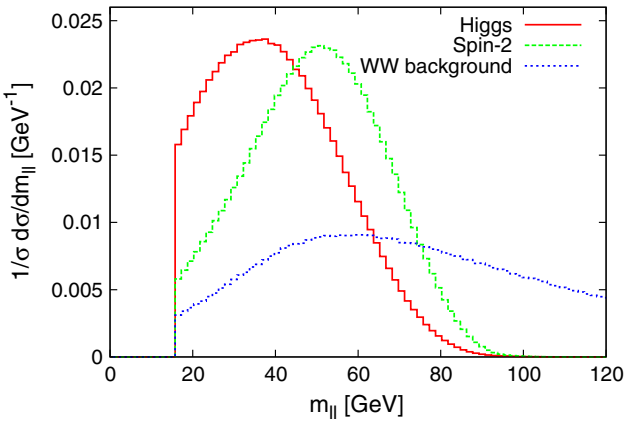

Fig. 6 Normalized distribution of the invariant di-lepton mass for $gg \to W^+W^- \to e^+\nu_e\,\mu^-\bar{\nu}_\mu$ for a SM Higgs and a spin-2 resonance with couplings $f_1 = 0.04$, $f_2 = 0.08$, $f_5 = 10$, $f_9 = 0.04$ at LO QCD accuracy and the di-boson-production background including $q\bar{q} \to WW$ at NLO QCD plus the continuum production diagrams of $gg \to WW$

spin-2 signal and the di-boson continuum, a precise knowledge of the background is necessary.

In Fig. 7, the model dependence of the invariant di-lepton-mass distribution is studied for the spin-0 and spin-2 case. As in the VBF mode (Fig. 5), this observable is nearly independent of the spin-2 coupling parameters, whereas anomalous Higgs couplings can have a certain effect. Since only the HWW couplings are relevant for the process $gg \to W^+W^-$, we only consider the first two terms of the Lagrangian 2.6 and we neglect the form factor. Whereas the $\mathcal{CP}$-even coupling g_{5e}^{HWW} alone (or the mixed case $g_{5e}^{HWW} = g_{5o}^{HWW}$) tend to shift the distribution to smaller values of m_{ll}, which facilitates the spin determination, the m_{ll}-distribution of a $\mathcal{CP}$-odd Higgs with g_{5o}^{HWW} is more similar to the one of a spin-2 resonance.

5 Conclusions

We have studied the characteristics of different spin-0 and spin-2 hypotheses in order to determine the spin of the new resonance discovered at the LHC. To this end, we have implemented an effective model, describing the interaction of a spin-2 particle with SM gauge bosons, into the Monte Carlo program VBFNLO. Comparing rates of spin-0 and spin-2 resonances produced in gluon fusion or vector-boson fusion in the decay modes $\gamma\gamma$, $W^+W^- \to 2l2\nu$ and $ZZ \to 4l$, we find that with a suitable choice of model parameters, a spin-2 resonance can approximately reproduce SM Higgs rates in the main detection channels. Likewise, transverse-momentum distributions of a spin-2 resonance can be adjusted to those of a SM Higgs by tuning form-factor parameters, leaving angular and invariant-mass distributions for a spin determination. In the VBF production mode, we found the azimuthal angle difference between the two tagging jets to be a very important variable to distinguish between spin-0 and spin-2. Its characteristics are nearly independent of spin-2 model parameters, NLO QCD corrections and decay mode, extending the range of applicability of the experimental results, which have mostly been obtained in the 2_m^+ scenario. Furthermore, in the $W^+W^- \to l^+\nu l^-\bar{\nu}$ decay, the invariant mass of the two charged leptons clearly distinguishes between spin-0 and spin-2 in VBF as well as in gluon fusion. Anomalous spin-0 scenarios, however, can lead to distributions which significantly differ from those of the SM Higgs. Therefore, it is important to carefully disentangle spin and $\mathcal{CP}$ properties of the new resonance. Since our default spin-2 model is largely compatible with present rate measurements at the LHC, we suggest that similar parametrizations, in particular $f_5 \gg f_1, f_2$, are used for further spin studies at the LHC as candidate spin-2 models.

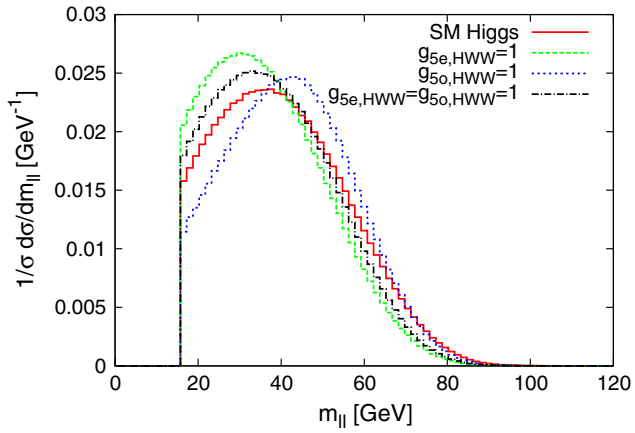

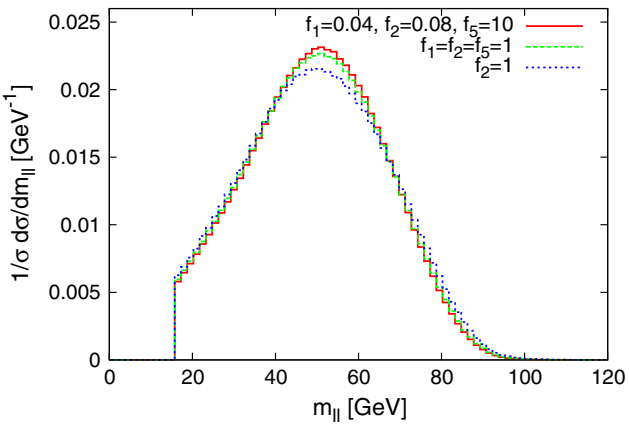

Fig. 7 Spin-0 and spin-2 model dependence of the invariant di-lepton mass in the gluon-fusion mode (LO QCD accuracy). *Left hand side* Higgs resonance with SM couplings, $\mathcal{CP}$-even and $\mathcal{CP}$-odd anomalous couplings; *right hand side* spin-2 resonance with different coupling parameters (always including $f_9 = 0.04$)

Acknowledgments We gratefully acknowledge F. Campanario's help in implementing the SM part of the gluon-fusion processes. This research was supported in part by the Deutsche Forschungsgemeinschaft via the Sonderforschungsbereich/Transregio SFB/TR-9 "Computational Particle Physics" and the Initiative and Networking Fund of the Helmholtz Association, contract HA-101("Physics at the Terascale"). J.F. acknowledges support by the "Landesgraduiertenförderung" of the State of Baden-Württemberg.

References

1. G. Aad et al. [ATLAS Collaboration], Phys. Lett. B **716**, 1 (2012)
2. S. Chatrchyan et al. [CMS Collaboration], Phys. Lett. B **716**, 30 (2012)
3. P.W. Higgs, Phys. Lett. **12**, 132 (1964)
4. P.W. Higgs, Phys. Rev. Lett. **13**, 508 (1964)
5. P.W. Higgs, Phys. Rev. **145**, 1156 (1966)
6. F. Englert, R. Brout, Phys. Rev. Lett. **13**, 321 (1964)
7. G.S. Guralnik, C.R. Hagen, T.W.B. Kibble, Phys. Rev. Lett. **13**, 585 (1964)
8. ATLAS Collaboration, ATLAS-CONF-2013-034
9. CMS Collaboration, CMS PAS HIG-13-005
10. S. Chatrchyan et al. [CMS Collaboration], Phys. Rev. Lett. **110**, 081803 (2013)
11. ATLAS Collaboration, ATLAS-CONF-2013-013
12. CMS Collaboration, CMS PAS HIG-13-002
13. ATLAS Collaboration, ATLAS-CONF-2013-031
14. CMS Collaboration, CMS PAS HIG-13-003
15. ATLAS Collaboration, ATLAS-CONF-2013-029
16. ATLAS Collaboration, ATLAS-CONF-2013-040
17. G. Aad et al. [ATLAS Collaboration], Phys. Lett. B **726**, 120 (2013). arXiv:1307.1432 [hep-ex]
18. S. Chatrchyan et al. [CMS Collaboration], JHEP **1401**, 096 (2014). arXiv:1312.1129 [hep-ex]
19. S. Chatrchyan et al. [CMS Collaboration]. arXiv:1312.5353 [hep-ex]
20. CMS Collaboration [CMS Collaboration], CMS-PAS-HIG-13-016
21. L.D. Landau, Dokl. Akad. Nawk., USSR **60**, 207 (1948)
22. C.N. Yang, Phys. Rev. **77**, 242 (1950)
23. J. Frank, M. Rauch, D. Zeppenfeld, Phys. Rev. D **87**, 055020 (2013)
24. S.Y. Choi, D.J. Miller, 2, M.M. Muhlleitner, P.M. Zerwas, Phys. Lett. B **553**, 61 (2003)
25. Y. Gao, A.V. Gritsan, Z. Guo, K. Melnikov, M. Schulze, N.V. Tran, Phys. Rev. D **81**, 075022 (2010)
26. C. Englert, C. Hackstein, M. Spannowsky, Phys. Rev. D **82**, 114024 (2010)
27. A. De Rujula, J. Lykken, M. Pierini, C. Rogan, M. Spiropulu, Phys. Rev. D **82**, 013003 (2010)
28. R. Boughezal, T.J. LeCompte, F. Petriello. arXiv:1208.4311 [hep-ph]
29. J. Ellis, D.S. Hwang, V. Sanz, T. You, JHEP **1211**, 134 (2012)
30. A. Alves, Phys. Rev. D **86**, 113010 (2012)
31. S.Y. Choi, M.M. Muhlleitner, P.M. Zerwas, Phys. Lett. B **718**, 1031 (2013)
32. C.-Q. Geng, D. Huang, Y. Tang, Y.-L. Wu, Phys. Lett. B **719**, 164 (2013)
33. C. Englert, D. Goncalves-Netto, K. Mawatari, T. Plehn, JHEP **1301**, 148 (2013)
34. S. Banerjee, J. Kalinowski, W. Kotlarski, T. Przedzinski, Z. Was, Eur. Phys. J. C **73**, 2313 (2013)
35. A. Djouadi, R.M. Godbole, B. Mellado, K. Mohan, Phys. Lett. B **723**, 307 (2013)
36. T. Modak, D. Sahoo, R. Sinha, H. -Y. Cheng. arXiv:1301.5404 [hep-ph]
37. X.-G. He, S.-F. Li, H.-H. Lin, Mod. Phys. Lett. A **28**, 1350085 (2013)
38. J. Ellis, V. Sanz, T. You, Eur. Phys. J. C **73**, 2507 (2013)
39. C. Englert, D. Goncalves, G. Nail, M. Spannowsky, Phys. Rev. D **88**, 013016 (2013)
40. D. Boer, W.J.d Dunnen, C. Pisano, M. Schlegel, Phys. Rev. Lett. **111**, 032002 (2013)
41. J. Ellis, V. Sanz, T. You, Phys. Lett. B **726**, 244 (2013)
42. S. Bolognesi, Y. Gao, A.V. Gritsan, K. Melnikov, M. Schulze, N.V. Tran, A. Whitbeck, Phys. Rev. D **86**, 095031 (2012)
43. J. Ellis, D.S. Hwang, JHEP **1209**, 071 (2012)
44. J. Ellis, R. Fok, D.S. Hwang, V. Sanz, T. You, Eur. Phys. J. C **73**, 2488 (2013)
45. K. Arnold, J. Bellm, G. Bozzi, F. Campanario, C. Englert, B. Feigl, J. Frank, T. Figy et al. arXiv:1207.4975 [hep-ph]
46. K. Arnold, J. Bellm, G. Bozzi, M. Brieg, F. Campanario, C. Englert, B. Feigl, J. Frank et al. arXiv:1107.4038 [hep-ph]
47. K. Arnold, M. Bahr, G. Bozzi, F. Campanario, C. Englert, T. Figy, N. Greiner, C. Hackstein et al., Comput. Phys. Commun. **180**, 1661 (2009)
48. T. Plehn, D.L. Rainwater, D. Zeppenfeld, Phys. Rev. Lett. **88**, 051801 (2002)
49. T. Figy, D. Zeppenfeld, Phys. Lett. B **591**, 297 (2004)
50. T. Figy, C. Oleari, D. Zeppenfeld, Phys. Rev. **D68**, 073005 (2003)
51. E.W.N. Glover, J.J. van der Bij, Phys. Lett. B **219**, 488 (1989)
52. C. Kao, D.A. Dicus, Phys. Rev. D **43**, 1555 (1991)
53. T. Binoth, M. Ciccolini, N. Kauer, M. Kramer, JHEP **0503**, 065 (2005)
54. T. Binoth, M. Ciccolini, N. Kauer, M. Kramer, JHEP **0612**, 046 (2006)
55. E.W.N. Glover, J.J. van der Bij, Nucl. Phys. B **321**, 561 (1989)
56. T. Binoth, N. Kauer, P. Mertsch. arXiv:0807.0024 [hep-ph]
57. T. Binoth, J.P. Guillet, E. Pilon, M. Werlen, Eur. Phys. J. C **16**, 311 (2000)
58. S. Dawson, Nucl. Phys. B **359**, 283–300 (1991)
59. D. Graudenz, M. Spira, P. Zerwas, Phys. Rev. Lett. **70**, 1372–1375 (1993)
60. R.V. Harlander, Phys. Lett. B **492**, 74–80 (2000)
61. S. Catani, D. de Florian, M. Grazzini, JHEP **05**, 025 (2001)
62. R.V. Harlander, W.B. Kilgore, Phys. Rev. D **64**, 013015 (2001)
63. R.V. Harlander, W.B. Kilgore, Phys. Rev. Lett. **88**, 201801 (2002)
64. C. Anastasiou, K. Melnikov, Nucl. Phys. B **646**, 220–256 (2002)
65. V. Ravindran, J. Smith, W.L. van Neerven, Nucl. Phys. B **665**, 325–366 (2003)
66. S. Catani, D. de Florian, M. Grazzini, P. Nason, JHEP **07**, 028 (2003)
67. J. Blümlein, V. Ravindran, Nucl. Phys. B **716**, 128–172 (2005)
68. S. Marzani, R.D. Ball, V. Del Duca, S. Forte, A. Vicini, Nucl. Phys. B **800**, 127–145 (2008)
69. R.V. Harlander, K.J. Ozeren, Phys. Lett. B **679**, 467–472 (2009)
70. A. Pak, M. Rogal, M. Steinhauser, Phys. Lett. B **679**, 473–477 (2009)
71. C. Anastasiou, R. Boughezal, F. Petriello, JHEP **04**, 003 (2009)
72. R.V. Harlander, K.J. Ozeren, JHEP **11**, 088 (2009)
73. R.V. Harlander, H. Mantler, S. Marzani, K.J. Ozeren, Eur. Phys. J. C **66**, 359–372 (2010)

74. A. Pak, M. Rogal, M. Steinhauser, JHEP **02**, 025 (2010)
75. D. de Florian, M. Grazzini, Phys. Lett. B **674**, 291 (2009)
76. LHC Higgs Cross Section Working Group. https://twiki.cern.ch/twiki/bin/view/LHCPhysics/CrossSections (SM Higgs production cross section in gluon fusion at 8 TeV based on [75])
77. S. Actis, G. Passarino, C. Sturm, S. Uccirati, Phys. Lett. B **670**, 12 (2008)
78. P. Artoisenet, P. de Aquino, F. Demartin, R. Frederix, S. Frixione, F. Maltoni, M.K. Mandal, P. Mathews et al., JHEP **1311**, 043 (2013)
79. T. Inami, T. Kubota, Y. Okada, Z. Phys, C **18**, 69 (1983)
80. A. Djouadi, M. Spira, P.M. Zerwas, Phys. Lett. B **264**, 440 (1991)
81. M. Spira, A. Djouadi, D. Graudenz, P.M. Zerwas, Nucl. Phys. B **453**, 17 (1995)
82. K. Nakamura et al. (Particle Data Group), J. Phys. G **37**, 075021 (2010)
83. J. Pumplin, D.R. Stump, J. Huston, H.L. Lai, P.M. Nadolsky, W.K. Tung, JHEP **0207**, 012 (2002)
84. H.-L. Lai, M. Guzzi, J. Huston, Z. Li, P.M. Nadolsky, J. Pumplin, C.-P. Yuan, Phys. Rev. D **82**, 074024 (2010)
85. M.H. Seymour, Nucl. Phys. B **513**, 269–300 (1998)
86. S. Frixione, Phys. Lett. B **429**, 369–374 (1998)
87. C. Oleari, D. Zeppenfeld, Phys. Rev. D **69**, 093004 (2004)
88. ATLAS Collaboration, ATLAS-CONF-2013-030.
89. ATLAS Collaboration. arXiv:1206.0756 [hep-ex]
90. ATLAS Collaboration, ATLAS-CONF-2013-009
91. CMS Collaboration, CMS PAS HIG-13-006